SSC18-VIII-04

Attitude Dynamics Modeling of Nanosatellites with Flexible Deployable Structures

Mandar A. Phadnis
Graduate Student, Aerospace Engineering Sciences
University of Colorado, Boulder, CO 80309
mandar.phadnis@colorado.edu

Faculty Advisors:
Marcin D. Pilinski
Research Associate, Laboratory for Atmospheric and Space Physics
Scott E. Palo
Professor, Colorado Center for Astrodynamics Research
University of Colorado, Boulder, CO 80309

ABSTRACT

Maxwell is a student built CubeSat scheduled for launch in 2021. The satellite is being designed to carry and deploy a large reflectarray antenna for in-orbit ground communication testing. This paper develops a general model of a satellite with deployable boom-like structures and analyzes the effects of flexing dynamics of such deployables on the attitude performance of a three-axis stabilized CubeSat. The deployables are modeled as point tip masses with stiffness and damping properties tailored to represent those of the actual booms. The model is simulated with typical CubeSat attributes, while the mass and natural frequency of the deployables is varied. Deviations from the nominal position of the deployable are studied under large attitude correction and slewing maneuvers to estimate transient and steady state performances. Influence of mass of the deployable on controller gain constraints is analyzed. The analysis is then applied to the Maxwell CubeSat in a deployed reflectarray antenna configuration to study in-orbit attitude control performance.

INTRODUCTION

CUBESAT missions have seen a rapid growth in their numbers in the past decade. Missions are being designed with widening scopes and increasingly complex capabilities. With advancing requirements, especially in communications and science applications, deployable antennas and scientific instruments are beginning to be used as CubeSat payloads[1,2]. Although these nanosatellites buses are scaled down significantly from their conventionally large and expensive spacecraft counterparts, their deployable payloads do not always scale accordingly[3]. Given the typical scale of a CubeSat, the deployables thus start to have a considerable impact on the satellites mass and moment of inertia, thus altering its dynamics. This makes it worthwhile to investigate the flexing effects of deployables on the attitude control performance of the satellite. One such application is the Maxwell 6U (approximately 20×30×10 cm) CubeSat being developed by University of Colorado, Boulder for the University Nanosatellite Program (UNP) administered by the Air Force Office of Scientific Research (AFOSR). Maxwell is being developed to achieve high rate data communication using CDMA technology on board a CubeSat. The Maxwell CubeSat was designed to fly and test a novel Deployable High Gain Reflectarray (DaHGR)[4] antenna which will employ a 1 m^2 reflectarray, having a considerable moment of inertia, compared to its host satellite. When deployed it will change the minimum principal inertia axis of the system to become the maximum principal inertia axis. This along with the pointing requirements (±3°) imposed during a ground pass slew maneuver motivated this research. The antenna structure to be deployed from a 2U (10×10×20 cm) component of Maxwell will consist of four main booms supporting a reflectarray antenna sheet. This X-band antenna will provide a higher gain, while enforcing stricter constraints on reference attitude tracking, due to its narrower beam width. This paper contains the results report of the effects of such deployable boom structures on the rotational dynamics of CubeSats which are otherwise largely treated as rigid bodies.

Rigid-flexible multibody dynamics are often extensively studied for large satellite missions usually with considerable resources to do so. Wu, et al.[5] models a large satellite antenna using modal analysis and provides an adaptive control approach to parametric uncertainties. Bai, et al.[6] use Lagrangian method to

develop first order approximation of the coupling deformation field. Alipour, et al.[7] decouples the rigid and flexible members and introduces floating frames for flexible members with reference and elastic variables. Wang, et al.[8] use finite element method to discretize flexible appendages. In contrast, the method developed in this paper has the properties of simplicity, scalability to other CubeSats and low dependence on flexible material parameters. CubeSat projects are often constrained on their resources and timeline and unable to conduct an in-depth study. They also lack the sophisticated infrastructure and test equipment to conduct a structural analysis.

The analysis presented in this paper intends to provide a fast and simple method to get a first-order insight into the multibody dynamics over a varied parameter space. Some of these parameters that affect the performance like the mass, stiffness and damping properties, will be varied and typical cases will be presented from an attitude dynamics standpoint. Finally, the analysis will be applied to the Maxwell CubeSat as a case study. The assumption made for this method of having the entire mass of the deployable concentrated at its tip, provides the worst-case for analysis of the system performance. This model can realistically apply to many small satellite missions besides Maxwell. The THEMIS spacecraft, for example, employs multiple deployed tip mass instruments including amplifiers and magnetometers to analyze electric and magnetic fields in plasma[9]. Although a higher fidelity can be achieved using distributed mass and finite element methods, it also increases the number of deployable parameters and

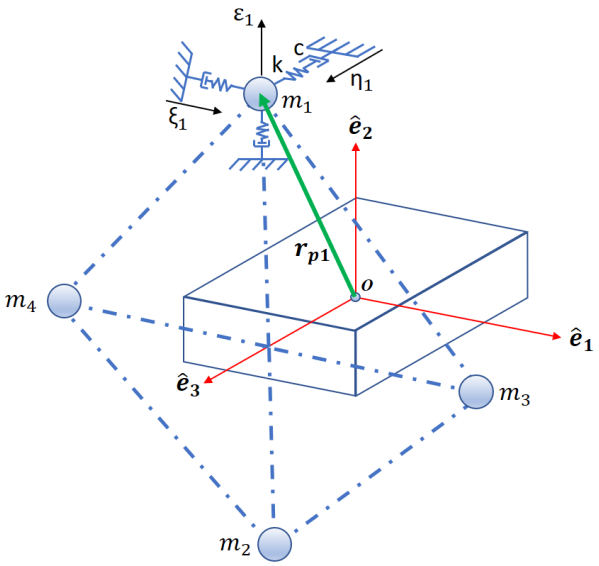

Figure 1: Satellite model with point tip mass deployables (Maxwell CubeSat configuration).

modeling resources needed to conduct such analysis. Whereas, this method can provide a fast, conservative, first pass estimate to assess feasibility of using a deployable structure with a given satellite.

SPACECRAFT MODEL DYNAMICS

The satellite is considered to be a rigid body with flexible deployable structures modeled as point masses having stiffness and damping properties, as shown in Fig. 1 below. The satellite body fixed frame $B:\{O:\underline{\hat{e}}_1,\underline{\hat{e}}_2,\underline{\hat{e}}_3\}$ is a right-handed co-ordinate system with its origin at the center of mass O and the axes aligned with the satellites principal axes of inertia. The mass moment of inertia matrix is then given as,

$$\left[I_{sat}\right]=\begin{bmatrix} I_{11} & I_{12} & I_{13} \\ I_{21} & I_{22} & I_{23} \\ I_{31} & I_{32} & I_{33} \end{bmatrix} \quad (1)$$

where the off-diagonal elements are zero for the given body frame. Each deployable structure is represented by a point mass (m_i) concentrated at its tip. This tip mass can have oscillations along the $\underline{\hat{e}}_1$, $\underline{\hat{e}}_2$ and $\underline{\hat{e}}_3$ principal body axes. The oscillatory displacement is assumed to be small and linearized along those axes. Fig. 1 shows this three-axis 'spring-mass-damper' model for mass m_1. The stiffness and damping can be varied along each of the axes. The instantaneous position of the i^{th} mass with respect to the satellites center of mass is given by $\underline{r}_{pi}$ in the body frame as,

$$\underline{r}_{pi}=(b_{1i}+\xi_i)\underline{\hat{e}}_1+(b_{2i}+\varepsilon_i)\underline{\hat{e}}_2+(b_{3i}+\eta_i)\underline{\hat{e}}_3 \quad (2)$$

where, $\underline{b}_i=\begin{bmatrix} b_{1i} & b_{2i} & b_{3i} \end{bmatrix}^T$ is the nominal location of the i^{th} tip mass in body frame, while ξ_i, ε_i and η_i are its oscillatory displacements along $\underline{\hat{e}}_1$, $\underline{\hat{e}}_2$ and $\underline{\hat{e}}_3$ respectively. This model can be extended to n deployables modeled as point masses at arbitrary locations in the body frame.

The satellite body attitude with respect to an inertial reference frame is defined using quaternions which describe the orientation of the satellite body axes with respect to inertial axes via a rotation through angle Φ, about principal rotation vector $\underline{\hat{p}}$ as[10],

$$\underline{q} = \begin{bmatrix} \cos(\Phi/2) & \sin(\Phi/2)\,\underline{\hat{p}} \end{bmatrix}^T \tag{3}$$

Total system mass in terms of the satellite mass m_{sat} and mass of the i^{th} point mass m_{pi} is given as,

$$M = m_{sat} + \sum_{i=1}^{n} m_{pi} \tag{4}$$

The first moment of inertia of the system is given as,

$$\underline{c} = \sum_{i=1}^{n} m_{pi}\,\underline{r}_{pi} \tag{5}$$

The instantaneous velocity of the center of mass can be calculated as[11],

$$\underline{v}_o = \left(\underline{c} \times \underline{\omega} - \sum_{i=1}^{n} (m_{pi}\,\dot{\xi}_i)\underline{\hat{e}}_1 - \sum_{i=1}^{n} (m_{pi}\,\dot{\varepsilon}_i)\underline{\hat{e}}_2 - \sum_{i=1}^{n} (m_i\,\dot{\eta}_i)\underline{\hat{e}}_3 \right) / M \tag{6}$$

where $\underline{\omega}$ is the satellite angular velocity vector in radians per second. The dynamic inertia matrix of the system is given by the equation,

$$[I_{sys}] = [I_{sat}] + \sum_{i=1}^{n} m_{pi} (\underline{r}_{pi}^{\,T}\,\underline{r}_{pi}[I_{3x3}] - \underline{r}_{pi}\,\underline{r}_{pi}^{\,T}) \tag{7}$$

The satellite angular momentum is derived to be[11],

$$\underline{h}_{sat} = \underline{h}_{sys} - \underline{c} \times \underline{v}_o - \sum_{i=1}^{n} (m_i\,\dot{\xi}_i(\underline{r}_{pi} \times \underline{\hat{e}}_1)) - \sum_{i=1}^{n} (m_i\,\dot{\varepsilon}_i(\underline{r}_{pi} \times \underline{\hat{e}}_2)) - \sum_{i=1}^{n} (m_i\,\dot{\eta}_i(\underline{r}_{pi} \times \underline{\hat{e}}_3)) \tag{8}$$

where $\underline{h}_{sys} = [I_{sys}]\underline{\omega}$. The linear momentum of i^{th} boom is given as

$$\underline{p}_i = m_i(\underline{v}_o + \underline{\omega} \times \underline{r}_{pi} + \dot{\xi}_i\,\underline{\hat{e}}_1 + \dot{\varepsilon}_i\,\underline{\hat{e}}_2 + \dot{\eta}_i\,\underline{\hat{e}}_3) \tag{9}$$

The states and rates are propagated using quaternion kinematics as[10],

$$\dot{\underline{q}} = \frac{1}{2}\Omega \bullet \underline{q} \tag{10}$$

where

$$\Omega = \begin{bmatrix} 0 & -\omega_1 & -\omega_2 & -\omega_3 \\ \omega_1 & 0 & \omega_3 & -\omega_2 \\ \omega_2 & -\omega_3 & 0 & \omega_1 \\ \omega_3 & \omega_2 & -\omega_1 & 0 \end{bmatrix} \tag{11}$$

The rate of change of angular momentum is related to the control torque $\underline{u}$ as,

$$\dot{\underline{h}}_{sys} = -\underline{\omega} \times \underline{h}_{sys} + \underline{u} \tag{12}$$

Tip mass linear acceleration along $\underline{\hat{e}}_1$, $\underline{\hat{e}}_2$ and $\underline{\hat{e}}_3$ axes is given as,

$$\dot{p}_{i1} = (\underline{\omega} \times \underline{\hat{e}}_1) \bullet \underline{p}_i - k_1\,\dot{\xi}_i - c_1\xi_i \tag{13.1}$$

$$\dot{p}_{i2} = (\underline{\omega} \times \underline{\hat{e}}_2) \bullet \underline{p}_i - k_2\,\dot{\varepsilon}_i - c_2\varepsilon_i \tag{13.2}$$

$$\dot{p}_{i3} = (\underline{\omega} \times \underline{\hat{e}}_3) \bullet \underline{p}_i - k_3\,\dot{\eta}_i - c_3\eta_i \tag{13.3}$$

where k_j and c_j are the stiffness and damping coefficients along the $\underline{\hat{e}}_j$ axis respectively.

Finally, the tip oscillations are propagated as,

$$\dot{\xi}_i = p_{i1}/m_i + \underline{\hat{e}}_1 \bullet (\underline{r}_{pi} \times \underline{\omega}) - \underline{\hat{e}}_1 \bullet \underline{v}_o \tag{14.1}$$

$$\dot{\varepsilon}_i = p_{i2}/m_i + \underline{\hat{e}}_2 \bullet (\underline{r}_{pi} \times \underline{\omega}) - \underline{\hat{e}}_2 \bullet \underline{v}_o \tag{14.2}$$

$$\dot{\eta}_i = p_{i3}/m_i + \underline{\hat{e}}_3 \bullet (\underline{r}_{pi} \times \underline{\omega}) - \underline{\hat{e}}_3 \bullet \underline{v}_o \tag{14.3}$$

The state vector for the following simulations was then built as given below

$$\underline{x} = \begin{bmatrix} \underline{q} & h_{sys} & \underline{p} & \underline{\xi} & \underline{\varepsilon} & \underline{\eta} \end{bmatrix}^T \tag{15}$$

Numerical integration was conducted using a variable step Runga-Kutta-Fehlberg method of order 4 and error

estimator order 5. The absolute and relative tolerance were set at 10^{-18}.

SIMULATION RESULTS

Two simulations were conducted employing the above described model. In the first subsection, a typical CubeSat is simulated and the parameters of its deployable, like the tip mass (affecting its natural frequency) are varied to analyze the effects under slewing maneuvers. Effect of the tip mass on control performance is also studied for large attitude corrections. The second subsection is based on a mission scenario expected by the Maxwell CubeSat with the deployable reflectarray antenna modeled as four tip masses as shown in Fig. 1.

Variation of deployable boom parameters

In this simulation, a CubeSat of mass 10 kg is considered. The deployable is modeled as a one and half meter boom with nominal position of its tip at $\underline{b}_1 = \begin{bmatrix} 1.5 & 0 & 0.2 \end{bmatrix}^T m$. Referring to Fig. 1, this would correspond to the location of mass m_3. It was assumed that the deployables are of fixed length and do not compress nor expand in length, under torque. Thus, to avoid oscillations of this tip mass along its length axis $\hat{\underline{e}}_1$, the corresponding stiffness and damping coefficients were adjusted for any motion along the length to be negligible. The tip mass of the deployable was varied from 0.15 kg to 2.5 kg, keeping stiffness and damping coefficients constant. The results were observed for a slew maneuver at 1 degree per second angular rate about the $\hat{\underline{e}}_2$ axis. Along with the time history, results were noted as peak transient and steady state displacements in the deployable tip as a function of its natural frequency. Fig. 2 gives the time history of the absolute displacement for some of the frequencies (as emulated by the tip mass motion). Transients for the graphed frequencies settled to steady state errors of the order of 10^{-3} degrees within 10 seconds for the designed control. The results in Fig. 3 show peak transient deflections of up to 0.07° for natural frequencies below 0.5 Hz. Fig. 4 shows steady state displacement as a function of natural frequency of the tip mass. The displacements are significant for natural frequencies below 0.5 Hz and the effects of sharply drop off above 1 Hz.

Another aspect that can be crucial during a feasibility analysis is controller stability and performance. In order to study the effects of a deployable on attitude control, a reaction wheel based nonlinear feedback controller was implemented following the feedback linearization method[10], tuned to

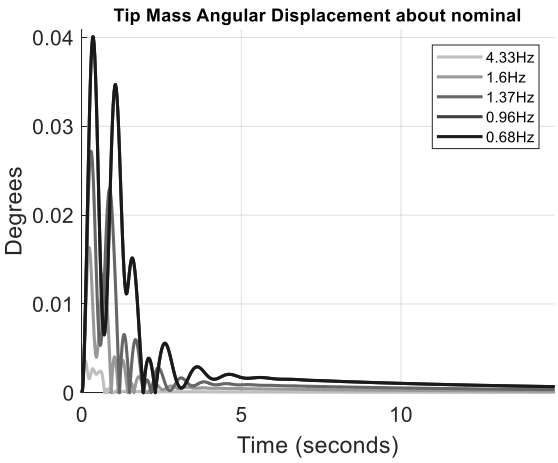

Figure 2: Absolute angular displacement of tip mass deployables per natural frequency.

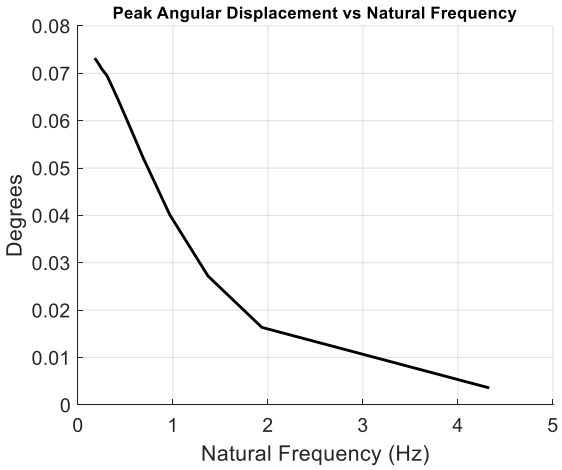

Figure 3: Peak transient angular displacement as a function of deployable natural frequency (1°/s slew maneuver).

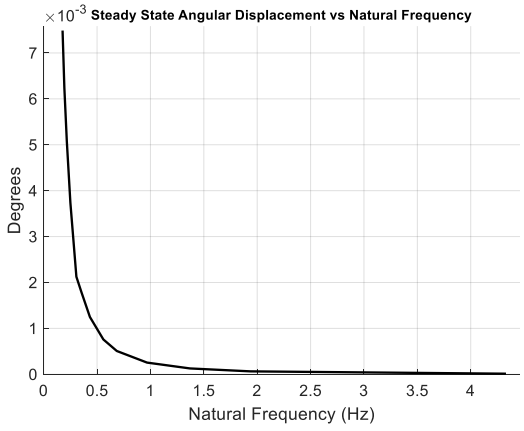

Figure 4: Steady state angular displacement as a function of deployable natural frequency (1°/s slew maneuver).

perform as a critically damped system and tested for a 180° rotation maneuver. This control performance was held as the baseline for comparing variations in settling time and overshoots as the tip mass was increased. The reaction wheels were modeled according to the commonly employed four reaction wheel redundant systems with a 6500 RPM limit, and 0.0032 Nm torque limit for each wheel. The weight of each tip mass was varied from 1.5% to 25% of that of the CubeSat rigid body for fixed stiffness and damping parameters. The effects on controller performance were graphed as presented in the Fig. 5 below. Peak overshoot and settling time were observed as a function of the percentage mass of the deployable payload compared to that of the CubeSat. Note that the first-derivative discontinuities in the plot are due to the control error angle being defined only from 0° to 180°. Results in

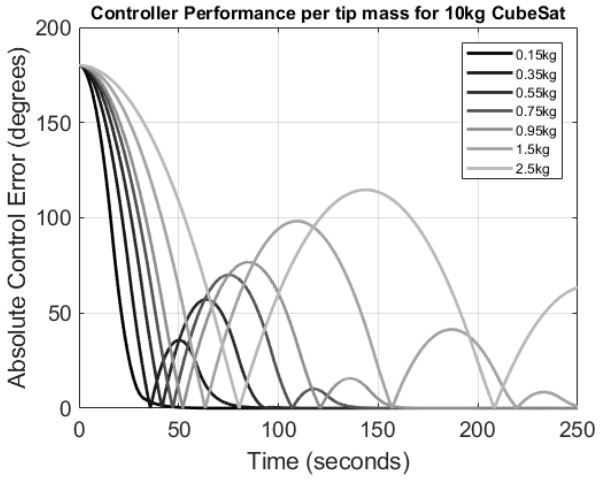

Figure 5: Controller performance per deployable tip mass.

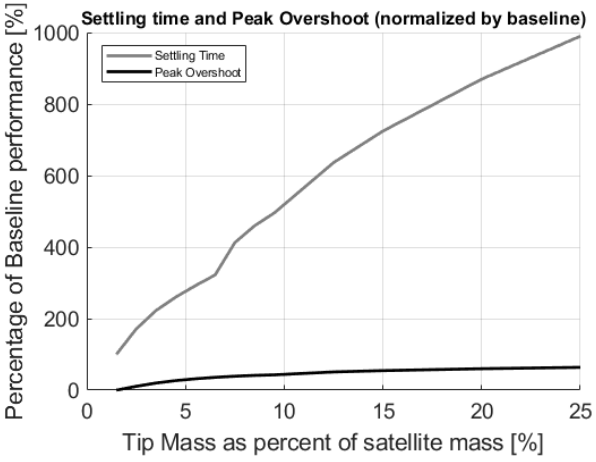

Figure 6: Percent increase in peak overshoot and settling time per deployable mass, compared to a critically damped baseline performance.

Figs. 5 and 6 indicate that the critically damped behavior is maintained for the 0.15 kg deployable, while effects of the deployed payloads on the control performance are minimal for masses less than 3.5% of the satellite mass. For masses over 3.5%, the controller shows increasingly underdamped behavior with large overshoots and longer settling times. As can be observed in Fig. 6, the effects on settling time are much more prominent than those on the overshoot. For a 0.95 kg deployable mass, the settling time of 160 seconds was more than 500% of the critically damped baseline performance. This is due to the underdamped behavior recursively setting the deployable into oscillations.

Maxwell CubeSat Case Study

In this section, we present simulation results for the Maxwell CubeSat with the reflectarray antenna. The CubeSat configuration with the antenna deployed is as shown in Fig. 1. The satellite mass is 7.121 kg, in a 6U configuration. The reflectarray antenna is primarily made up of four booms and is mounted with its axis of symmetry along the minimum inertia axis of the satellite. The satellite's principal moments of inertia in the body frame are $I_{sat} = [0.1614 \quad 0.1854 \quad 0.1397]\, kg.m^2$ prior to reflectarray deployment, whereas after deployment those of the satellite-reflectarray system are $I_{sys} = [2.4914 \quad 2.5154 \quad 4.6397]\, kg.m^2$. The boom parameters such as mass, length, natural frequency and damping were used as provided by the antenna manufacturer. The system is tested under various expected mission conditions. The most important being the ground pass slew, which had the strictest pointing constraints on the antenna of within 3°. Fig. 7 shows the first 400 seconds of the 10-minute long, 1°/s slewing maneuver. The graph illustrates the absolute

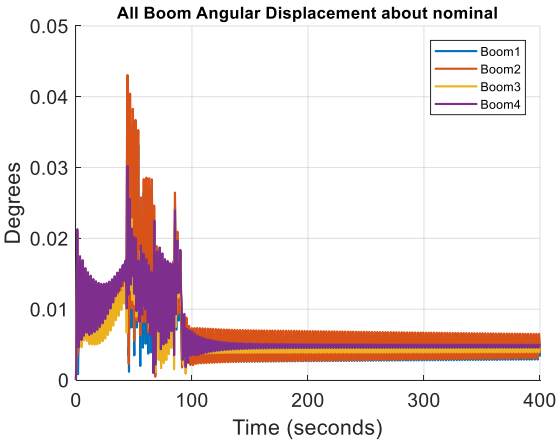

Figure 7: Boom displacements in deployable antenna (1°/s slew maneuver) with high control gains.

angular displacements in degrees of the 4 tip masses about their nominal locations. The maximum transient displacement among the antenna booms was over 0.04°. The steady state oscillations during the slew were within 0.008° for the designed control gains. These sustained oscillations were due to the continuous control torque being applied to track a rotating target reference frame.

To improve the steady state performance, the control gains were reduced during the slew. Fig. 8 below shows the same 1°/s slew maneuver, which now ends at the 300 second mark. It shows the dynamics of the deployable structure when the control goes from slewing to inertial pointing. As the slewing ends and the

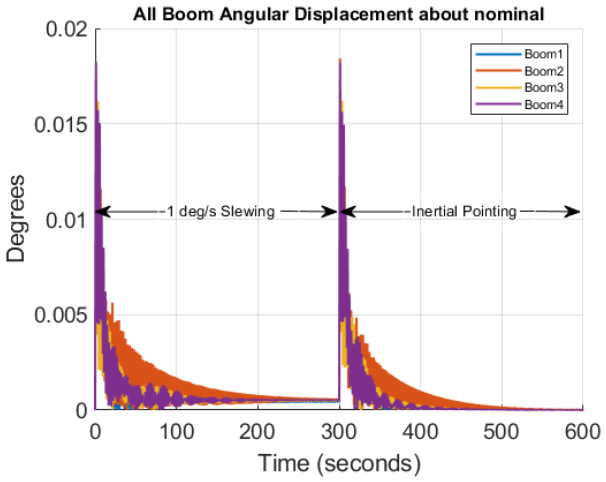

Figure 8: Boom displacements in deployable antenna (1°/s slew maneuver followed by inertial pointing) with low control gains.

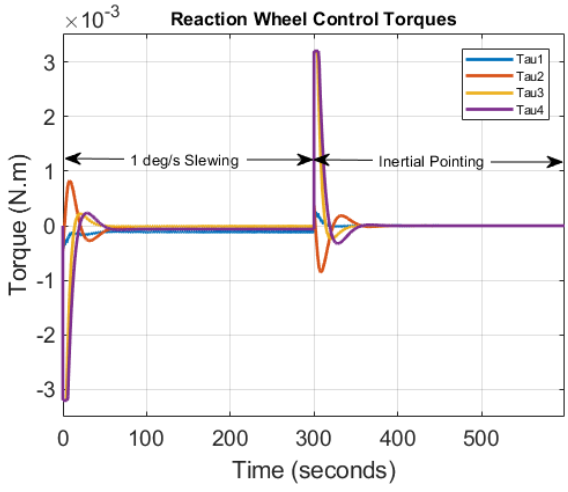

Figure 9: Reaction wheel control torques (1°/s slew maneuver followed by inertial pointing) with low control gains.

control holds the satellite inertially to its final slew attitude, transients are set off which settle to zero over the next 150 seconds. With the reduced control gains, the transient deflections were below 0.02°, whereas the steady state deflections were within 0.0005°. Fig. 9 shows the reaction wheel control torques for this case. Given the mission requirements and pointing budget for Maxwell CubeSat, this was well within the performance constraints.

CONCLUSION

A low cost and simple method to analyze effects of large deployables on nanosatellites has been investigated by modeling the deployables as tip masses with stiffness and damping properties. Simulations of this model provided insights into transient and steady state pointing errors of the deployables under large attitude corrections and slewing maneuvers over varied parameters. The transient errors were found to be significant under 0.5 Hz natural frequency of the deployable. The effects were also analyzed from a controller performance standpoint. It was found that it becomes worthwhile to consider dynamics of flexing deployables towards controller gain constraints, especially when their mass exceeds 5% of the satellite mass. This method can be used in controller gain retuning for a pre- to post-deployment satellite configuration. Ignoring deployable masses over this range may cause unexpected control performance or even stability concerns. This analysis was applied to Maxwell CubeSat to evaluate the feasibility of using a large deployable reflectarray antenna to improve its communication capabilities. The analysis was conducted for expected mission scenarios and the attitude control gains were adjusted post deployment so that the performance was within the control design and ground communication requirements.

REFERENCES

Papers

1. Joseph, A., Deshpande, M., O'Neil, P., Miles, L., "Development of VHF (240–270 MHz) Antennas for SoOp (Signal of Opportunity) Receiver for 6U CubeSat Platforms", 2016 Progress in Electromagnetic Research Symposium (PIERS), Shanghai, China, Aug. 2016.
2. R. W. Conversano, R. E. Wirz, "Mission Capability Assessment of CubeSats Using a Miniature Ion Thruster", Journal of Spacecraft and Rockets, Vol. 50, No. 5, September–October 2013.
3. Belvin, W., Straubel, M., et al., "Advanced deployable structural systems for small satellites", NATO CSO STO Meeting on Best

Practices for Risk Reduction for Overall Space Systems, Zaragoza, Spain, 26-30 Sep. 2016.

4. P. Keith Kelly, "A Scalable Deployable High Gain Antenna – DaHGR", 30th Annual AIAA/USU Conference on Small Satellites, Logan, UT, Aug. 2016.
5. Wu, S., Liu, Y., Radice, G., Tan, S., "Autonomous Pointing Control of a Large Satellite Antenna Subject to Parametric Uncertainty", MDPI, Basel, Switzerland, March 2017.
6. Bai, S., Huang, X., Liu, Y., "Dynamic Modeling and Simulation of a Flexible Satellite", IEEE 7th International Conference on System Simulation and Scientific Computing, Beijing, China, 2008.
7. Alipour, K., Zarafshan, P., Ebrahimi, A., "Dynamics modeling and attitude control of a flexible space system with active stabilizers", Nonlinear Dynamics, Vol. 84, Issue 4, Pg. 2535–2545, Springer, 2016.
8. Wang, J., Li, D., Jiang, J., "First order coupled dynamic model of flexible space structures with time-varying configurations", Acta Astronautica, Vol. 132, Pg. 117–123, March 2017.
9. Auslander, D., et al., "Instrument Boom Mechanisms on the THEMIS; Magnetometer, Radial Wire, and Axial Booms", Space Science Review, Vol. 141, Pg. 185-211, June 2008.

Books

10. Schaub, H., and Junkins, J. L., "Analytical Mechanics of Space Systems, 3rd ed.", AIAA Education Series, Virginia, 2014, Chs. 3, 8.
11. Hughes, P. C., "Spacecraft Attitude Dynamics", Wiley, New York, 1986, Chs. 3, 4.